Optical properties and magnetochromism in multiferroic BiFeO₃

X. S. Xu,[1] T. V. Brinzari,[1] S. Lee,[2] Y. H. Chu,[3] L. W. Martin,[3,4] A. Kumar,[5] S. McGill,[6] R. C. Rai,[1,*] R. Ramesh,[3,4]
V. Gopalan,[5] S. W. Cheong,[2] and J. L. Musfeldt[1]

[1]*Department of Chemistry, University of Tennessee, Knoxville, Tennessee 37996, USA*

[2]*Rutgers Center for Emergent Materials and Department of Physics, Rutgers University, Piscataway, New Jersey 08854, USA*

[3]*Department of Materials Science and Engineering, University of California, Berkeley, Berkeley, California 94720, USA*

and Department of Materials Science and Engineering, National Chiao Tung University, HsinChu, Taiwan 30010

[4]*Materials Science Division, Lawrence Berkeley National Laboratory, Berkeley, California 94720, USA*

[5]*Department of Materials Science and Engineering, Pennsylvania State University, University Park, Pennsylvania 16802, USA*

[6]*National High Magnetic Field Laboratory, Tallahassee, Florida 32310, USA*

In order to investigate spin-charge coupling in multiferroic oxides, we measured the optical properties of BiFeO₃. Although the direct 300 K charge gap is observed at 2.67 eV, absorption onset actually occurs at much lower energy with Fe^{3+} excitations at 1.41 and 1.90 eV. Temperature and magnetic-field-induced spectral changes reveal complex interactions between on-site crystal-field and magnetic excitations in the form of magnon sidebands. We employ the sensitivity of these magnon sidebands to map out the magnetic-field-temperature phase diagram which demonstrates optical evidence for spin spiral quenching above 20 T and suggests a spin domain reorientation near 10 T.

The interplay between charge, structure, and magnetism is the origin of rich physics in complex oxides. Because these interactions are so strong, oxides straddle several competing regions of physical, chemical, and size-shape phase space. An important consequence of this phase proximity is the physical property tunability and, in some cases, the opportunity to drive new functionality via modification of important energy and length scales in a material. Optical spectroscopy is a well-known probe of charge and bonding in solids. When charge and spin degrees of freedom are strongly coupled, it is also sensitive to magnetic excitations and spin ordering transitions.[1,2] Magnetochromism, the modification of a material's optical constants with applied magnetic field,[3,4] is an especially important tool for understanding magnetoelectric and multiferroic materials,[5,6] for which spin-charge interaction is expected to be large.

In this work, we focus on bismuth ferrite, the only single phase room-temperature multiferroic. This rhombohedrally distorted perovskite[7] is ferroelectric below 1100 K (T_c) due to Bi center displacement and a *G*-type antiferromagnet below 640 K (T_N).[7] BiFeO₃ is a correlated oxide with a 2.67 eV charge gap and electronic properties that are governed by strong hybridization and the Bi lone pair.[8,9] Bulk BiFeO₃ displays a spatially modulated spin arrangement ($\lambda \approx 620$ Å) due to the coexistence of electric and magnetic order and the coupling between electric polarization and spin.[10] These spin spirals persist up to T_N and disappear in a strong magnetic field ($H_C \approx 20$ T at 4 K).[7,11] Due to the robust electric and magnetic order, large polarization (~ 100 μC/cm²), photoferroelectric coupling, and tunable band gap, this polar oxide is attracting attention for energy harvesting applications.[12,13]

In order to investigate the interplay between charge and magnetism, we measured the optical and energy-dependent magneto-optical properties of multiferroic BiFeO₃ and compare our spectral results to first-principles electronic structure calculations,[8,9] the response of two similar ferrites (Fe₂O₃

and GaFeO₃),[14–17] and recent second harmonic generation experiments.[18] Temperature and magnetic-field-induced spectral changes reveal complex couplings between Fe^{3+} crystal-field and magnetic excitations in the form of magnon sidebands. We employ the sensitivity of these magnon sidebands to generate a magnetic-field-temperature phase diagram which displays spin spiral quenching at 20 T and suggests a spin domain reorientation at 10 T. These results demonstrate that charge dynamics coupled with static magnetic order is an excellent probe of $H-T$ phase space.

Rhombohedral single crystals with a $(012)_{hex}$ face were grown by flux techniques. Both thick (0.5 mm) and thin (67 μm) crystals were studied. A 500 nm rhombohedrally (111) oriented thin film deposited on a (111) SrTiO₃ substrate was also used. Transmittance experiments employed the 67 μm single crystal and the 500 nm thin film. The absorption coefficient $\alpha(E)$ was calculated directly from transmittance.[19] Near-normal reflectance experiments used the 0.5 mm thick crystal and a Kramers-Kronig analysis to determine the optical constants.[19] Measurements covered a wide range of energy (30 meV–6.5 eV), temperature (4–300 K) and magnetic field (0–33 T), employing a series of spectrometers in our own laboratory and at the NHMFL.[6] Absorption difference spectra emphasize small changes: $\Delta \alpha = \alpha(E,H) - \alpha(E,H=0$ T) at fixed temperature.

Figure 1 displays the 300 K absorption spectrum of BiFeO₃. Here, we employed a combination of samples and techniques to obtain the most reliable results across the full energy range of our investigation. This effort was necessary because the value of $\alpha(E)$ varies by 3 orders of magnitude between 1 and 6 eV.[20] We assign the observed excitations based on recent first-principles calculations[8,9] and by comparison with similar results in Fe₂O₃ and GaFeO₃.[15–17] Dipole-allowed excitations appear above 2.2 eV as O *p* to Fe *d* charge transfer in the minority channel. Features at higher energy are majority channel charge transfer excitations from strongly hybridized O *p* and Fe *d* states to Bi *p*
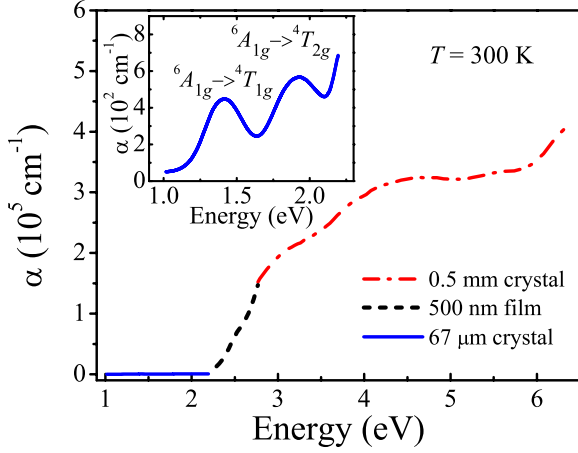
FIG. 1. (Color online) 300 K absorption coefficient $\alpha(E)$ as a function of energy. Inset: closeup view of $\alpha(E)$ below 2.2 eV. Although this data was collected from a series of samples, $\alpha(E)$ is an optical constant of the material.

FIG. 2. (Color online) (a) Variable temperature absorption spectra in the range of the Fe^{3+} $d-d$ excitations. (b) Oscillator strength (1–1.62 eV) as a function of temperature. Analysis of the 1.9 eV peak shows the same trends, but reliability is reduced due to overlap with the nearby charge transfer edge.

states. Via plots of $(\alpha E)^2$ vs E, we extract a 300 K optical gap of 2.67 eV,[13] in excellent agreement with recent ellipsometry data.[21–23] While the charge gap is at 2.67 eV, the onset of optical excitations is at lower energy. A shoulder centered near 2.5 eV [on the leading edge of $\alpha(E)$] has been discussed previously.[13] Furthermore, a closeup view of $\alpha(E)$ below 2.2 eV (inset, Fig. 1) shows two peaks centered at 1.41 and 1.90 eV and an overall level that is 3 orders of magnitude smaller than that above the charge gap. Both peak positions and the low oscillator strength are consistent with assignment as on-site Fe^{3+} crystal-field transitions. Following previous work on Fe_2O_3 and $GaFeO_3$, we attribute these peaks to $^6A_{1g} \rightarrow {}^4T_{1g}$ and $^6A_{1g} \rightarrow {}^4T_{2g}$ excitations.[15–17] Formally, these excitations are forbidden because they change the total spin of Fe^{3+} from $S=5/2$ to $S=3/2$. Spin-orbit coupling, however, relaxes the spin selection rule, giving rise to the small oscillator strengths observed here. The small octahedral distortion that breaks the parity selection rule makes it likely that the observed on-site excitations benefit from hybridization and are assisted by vibronic interactions involving odd-parity phonons.[14,15]

Figure 2(a) shows a close up view of the Fe^{3+} crystal-field excitations in $BiFeO_3$, the assignment of which is supported by an oscillator strength analysis. Taking the $^6A_{1g} \rightarrow {}^4T_{1g}$ excitation as an example, we calculate oscillator strength using the partial sum rule: $f \equiv \frac{2c}{N_e \hbar \pi \omega_p^2} \int_{E_1}^{E_2} n\alpha dE$. Here, $N_e=5$ is the number of electrons per Fe site, $n=2.7$ is the refractive index,[22] ω_p is the plasma frequency $\equiv \sqrt{\frac{e^2\rho}{m\epsilon_0}}$, e and m are the charge and mass of an electron, ϵ_0 is the vacuum dielectric constant, ρ is the density of Fe sites, c is the speed of light, and E_1 and E_2 are the energies of integration.[24] Overall f follows phonon activation trends, described by $f(T) = f_0(1+e^{-\hbar\omega/k_BT})$, where f_0 is the oscillator strength at temperature $T=0$ K and ω is the average phonon frequency.[14,15] This behavior indicates that vibronic excitations are dominant.[25] From intensity and width considerations, we estimate $\hbar\omega \sim 40$ meV and a Huang-Rhys electron-phonon coupling strength $S_H \sim 3$, indicative of intermediate
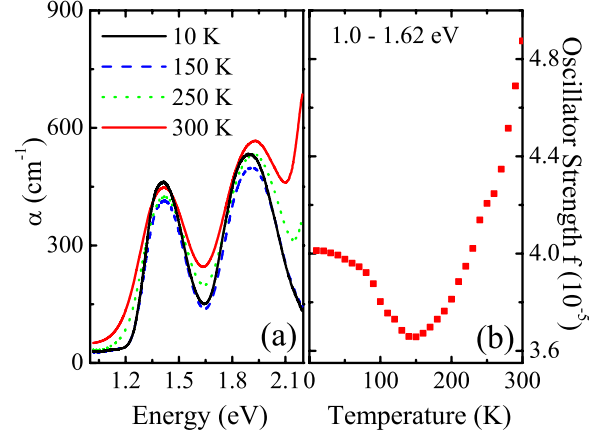
coupling.[25] Since $f_0 \propto 1-e^{-S_H}$, a change in S_H may account for the 150 K anomaly. In this case, increasing T increases $(1+e^{-\hbar\omega/k_BT})$ but decreases f_0, resulting a minimum at 150 K. Raman scattering highlighted a similar anomaly near 140 K which was interpreted as a spin reorientation transition.[26,27] Sizable oscillator strength changes in $BiFeO_3$ [Fig. 2(b)] vs modest changes at the Morin transition in Fe_2O_3 seem to rule out magnetic reorientation scenarios.[14]

Figure 3 displays the field-induced absorption difference spectra of $BiFeO_3$, $\Delta\alpha(E,H) \equiv \alpha(E,H)-\alpha(E,H=0)$, and data extracted from these absorption coefficient changes at selected energies and temperatures. This magnetochromic response demonstrates that Fe^{3+} d to d crystal-field excitations are intrinsically coupled to the microscopic spin structure. Three peaks (P_1, P_3, and P_4) and four dips (D_1 to D_4) can be identified [Fig. 3(a)]. As shown in Table I, these features can be grouped into pairs with similar $E_{Dip}^{\Delta\alpha}$-$E_{Peak}^{\Delta\alpha}$ energy differences. As illustrated in Fig. 3(a), the pattern in $\Delta\alpha(E,H)$ and the energy differences in Table I can be simulated by the displacement of four model oscillators (M_1 to M_4) with magnetic field. Strikingly, the model oscillator positions (E_{Peak}^α) do not match the main peaks in $\alpha(E)$, indicating that they have a different origin than the vibronic excitations discussed previously. As detailed below, we assign M_1 to M_4 as magnon sidebands of the pure electronic excitations.[2,28] Simple simulations of intensity and sideband displacement are in line with this assignment.

As depicted in Fig. 3(b), magnon sidebands can be viewed as crystal-field excitations on a Fe^{3+} site assisted by spin tilting on a neighboring site in a different spin sublattice that interact due to exchange interactions. In this case, both spin and parity selection rules are satisfied because the total spin is conserved and the initial and final states have different parities.[29] The shape of the magnon sidebands represents the joint density of states of pure crystal-field exciton and magnons, for which the peak positions correspond to zone boundary energies, due to the high density of states there, different from the zone center magnon observed in Raman scattering.[26,27]
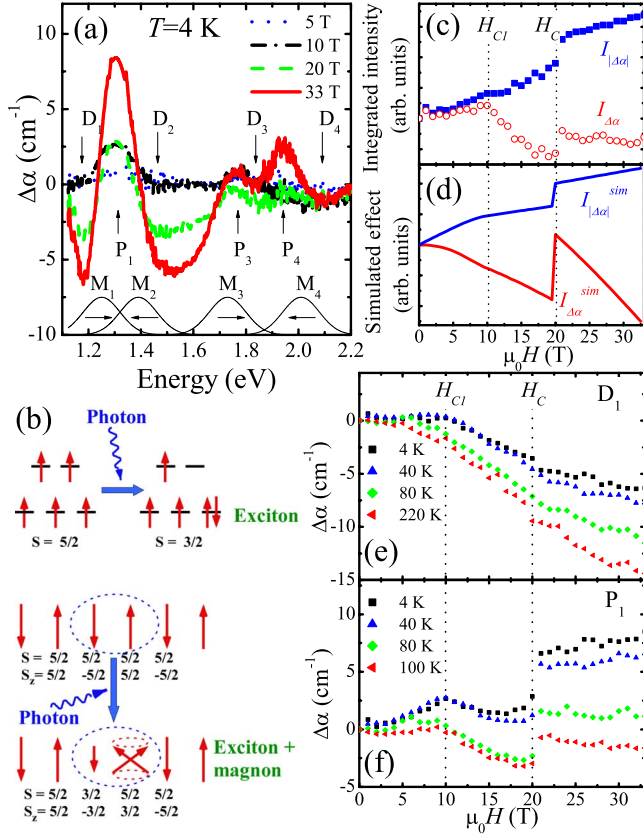
FIG. 3. (Color online) (a) $\Delta\alpha(E,H)$ for different magnetic fields at 4 K ($\vec{H} \perp (012)_{hex}$ face). Dips and peaks highlight magnon sideband displacements with field. Thin lines show proposed magnon peaks in $\alpha(E)$ that shift to generate the observed shape of $\Delta\alpha(E,H)$. Similar results are observed at higher temperatures. (b) Schematic illustration of magnon sidebands. The exciton and magnon are created together to satisfy selection rules. (c) Integrated absorption intensity (see text). (d) Simulated total intensity change $I_{\Delta\alpha}^{sim}(H) \propto -\Sigma\vec{S}_i \cdot \vec{S}_j$ and displacement $I_{|\Delta\alpha|}^{sim}(H) \propto \Sigma\vec{S}_i \cdot \vec{H}$ of magnon sidebands. (e) $\Delta\alpha$ as a function of magnetic field for D_1 at various temperatures. (f) $\Delta\alpha$ as a function of magnetic field for P_1 at various temperatures.

The microscopic origin of M_1 to M_4 and the essential characteristics of the absorption difference spectra, $\Delta\alpha(E,H)$, can be understood within the following scenario. Due to the rhombohedral distortion and local C_{3v} symmetry, the $^4T_{1g}$ and $^4T_{2g}$ states split into A_2+E and A_1+E levels, respectively. This reduced symmetry also yields two magnon peaks (M_1 and M_2) associated with the $^6A_{1g} \rightarrow {}^4T_{1g}$ excitation and two magnon peaks (M_3 and M_4) associated with the

TABLE I. Energies (in eV) of features in the 4 K $\Delta\alpha(E,H$ =33 T) spectra [Fig. 3(a)] related to magnon sidebands.

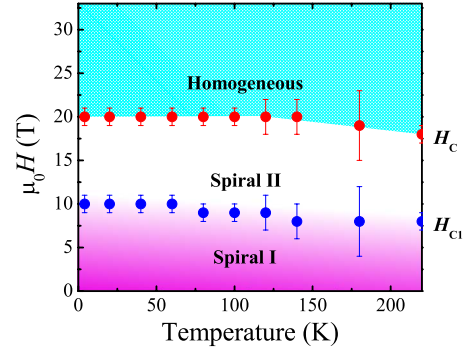|	$E_{Dip}^{\Delta\alpha}$	$E_{Peak}^{\Delta\alpha}$	$E_{Dip}^{\Delta\alpha}-E_{Peak}^{\Delta\alpha}$	E_{Peak}^{α}
$^6A_{1g} \rightarrow {}^4T_{1g}$	1.18(D_1)	1.31(P_1)	−0.13	1.25(M_1)
	1.47(D_2)	1.31(P_1)	0.16	1.39(M_2)
$^6A_{1g} \rightarrow {}^4T_{2g}$	1.66(D_3)	1.80(P_3)	−0.14	1.73(M_3)
	2.08(D_4)	1.94(P_4)	0.14	2.01(M_4)

FIG. 4. (Color online) $H-T$ phase diagram of BiFeO$_3$ constructed using $\Delta\alpha(E,H)$ data like that in Figs. 3(e) and 3(f).

$^6A_{1g} \rightarrow {}^4T_{2g}$ excitation. It is well known that magnon sidebands change position and intensity in a magnetic field.[29,30] In contrast, vibronic excitations are less sensitive to applied field. Because spin antialignment favors magnon sidebands, sideband intensity is proportional to $-\Sigma\vec{S}_i \cdot \vec{S}_j$, as a first-order approximation, where $\vec{S}_i$ ($\vec{S}_j$) is the spin on the ith (jth) Fe site. Since magnetic field tends to cant spins, an applied field generally reduces magnon sideband intensity. In addition, a magnetic field displaces magnon sidebands due to combined Zeeman effects and profile shape modifications, an effect roughly proportional to $\Sigma\vec{S}_i \cdot \vec{H}$.

To quantify magnon sideband behavior in magnetic field, we calculated $I_{\Delta\alpha}(H) \equiv \int_{1.1 \text{ eV}}^{2.2 \text{ eV}} \Delta\alpha(E,H)dE$ and $I_{|\Delta\alpha|}(H) \equiv \int_{1.1 \text{ eV}}^{2.2 \text{ eV}} |\Delta\alpha(E,H)|dE$. These quantities represent the total intensity change and displacement of the magnon sidebands, respectively [Fig. 3(c)]. Overall, $I_{\Delta\alpha}(H)$ decreases and $I_{|\Delta\alpha|}(H)$ increases, as expected. Interestingly, there are anomalies at H_C=20 T and H_{C1}=10 T. H_C corresponds to the well-known spin spiral to homogeneous antiferromagnetic transition.[7,11] A sharp increase in $I_{\Delta\alpha}(H)$ is observed because the transition enhances spin antialignment. The jump in $I_{|\Delta\alpha|}(H)$ comes from alignment of the weak ferromagnetic moment due to spin spiral quenching. The origin of H_{C1} is still an open question, although it was observed previously in electron spin resonance (and possibly magnetization) experiments.[7] Magnon sideband behavior suggests that the spiral planes may rotate in the field along the polarization $\vec{P}$, becoming perpendicular to the $\vec{P} \times \vec{H}$ plane, which is the lowest energy configuration.[7] This scenario is consistent with a more negative slope of $I_{\Delta\alpha}(H)$ for $H > H_{C1}$, because the effect of the magnetic field is larger when the spiral planes are perpendicular to $\vec{P} \times \vec{H}$ plane. On the other hand $I_{|\Delta\alpha|}(H)$ has a slight positive slope when $H < H_{C1}$ due to alignment of the weak ferromagnetic moment. Using this model, the behavior of magnon sidebands can be qualitatively reproduced, as shown in Fig. 3(d). H_{C1} may therefore represent an energy scale for overcoming the anisotropy barrier for rotation of the spiral plane. The order of magnitude of H_{C1} is in line with theoretical predictions.[31]

Combining our $\Delta\alpha(E,H)$ data at various temperatures [Figs. 3(e) and 3(f)], we construct the magnetic-field-temperature phase diagram of BiFeO$_3$ (Fig. 4). Two critical fields are observed. As expected, the magnitudes of both

critical fields decrease with temperature because elevated temperature weakens magnetic order. H_C corresponds to the transition from spin spiral antiferromagnetic to homogeneous antiferromagnetic phase.[7] As discussed previously, H_{C1} may be related to the rotation of the spiral plane. These results demonstrate that the optical properties of $BiFeO_3$ are sensitive to changes in field-induced spin structure.

Summarizing, we investigated the optical properties of $BiFeO_3$, a 300 K single phase multiferroic, of interest for fundamental cross-coupling studies and device applications. Although the 300 K charge gap is observed at 2.67 eV, absorption onset actually occurs at much lower energy with Fe^{3+} crystal-field excitations at 1.41 and 1.90 eV. In addition to unusual temperature trends in the oscillator strength, energy-dependent changes in $\Delta\alpha$ are observed when the magnetic field is applied. Magnetic sidebands are assigned according to their sensitivity to applied field. From the magnetochromic response, we generate an $H-T$ phase diagram which displays a quenching of the spin spiral above 20 T and suggests a 10 T spin domain reorientation. That magnon sidebands are sensitive to field-driven changes in the spin structure suggests future opportunities to investigate polar oxides.

*Department of Physics, Buffalo State College, Buffalo, NY 14222, USA.

[1] A. Pimenov, A. A. Mukhin, V. Y. Ivanov, V. D. Travkin, A. M. Balbashov, and A. Loidl, Nat. Phys. **2**, 97 (2006).

[2] R. L. Greene, D. D. Sell, W. M. Yen, and A. L. Schawlow, Phys. Rev. Lett. **15**, 656 (1965).

[3] J. Choi, J. D. Woodward, J. L. Musfeldt, X. Wei, M. H. Whangbo, J. He, R. Jin, and D. Mandrus, Phys. Rev. B **70**, 085107 (2004).

[4] J. Cao, J. T. Haraldsen, R. C. Rai, S. Brown, J. L. Musfeldt, Y. J. Wang, X. Wei, M. Apostu, R. Suryanarayanan, and A. Revcolevschi, Phys. Rev. B **74**, 045113 (2006).

[5] M. Fiebig, J. Phys. D **38**, R123 (2005).

[6] X. S. Xu, M. Angst, T. V. Brinzari, R. P. Hermann, J. L. Musfeldt, A. D. Christianson, D. Mandrus, B. C. Sales, S. McGill, J. W. Kim, and Z. Islam, Phys. Rev. Lett. **101**, 227602 (2008).

[7] A. M. Kadomtseva, A. K. Zvezdin, Y. F. Popov, A. P. Pyatakov, and G. P. Vorob'ev, JETP Lett. **79**, 571 (2004).

[8] J. B. Neaton, C. Ederer, U. V. Waghmare, N. A. Spaldin, and K. M. Rabe, Phys. Rev. B **71**, 014113 (2005).

[9] S. J. Clark and J. Robertson, Appl. Phys. Lett. **90**, 132903 (2007).

[10] I. Sosnowska, T. Peterlin-Neumaier, and E. Steichele, J. Phys. C **15**, 4835 (1982).

[11] R. Przenioslo, A. Palewicz, M. Regulski, I. Sosnowska, R. M. Ibberson, and K. S. Knight, J. Phys.: Condens. Matter **18**, 2069 (2006).

[12] D. Lebeugle, D. Colson, A. Forget, M. Viret, P. Bonville, J. F. Marucco, and S. Fusil, Phys. Rev. B **76**, 024116 (2007).

[13] S. R. Basu, L. W. Martin, Y. H. Chu, M. Gajek, R. Ramesh, R. C. Rai, X. Xu, and J. L. Musfeldt, Appl. Phys. Lett. **92**, 091905 (2008).

[14] L. A. Marusak, R. Messier, and W. B. White, J. Phys. Chem. Solids **41**, 981 (1980).

[15] A. I. Galuza, A. B. Beznosov, and V. V. Eremenko, Low Temp. Phys. **24**, 726 (1998).

[16] J. H. Jung, M. Matubara, T. Arima, J. P. He, Y. Kaneko, and Y. Tokura, Phys. Rev. Lett. **93**, 037403 (2004).

[17] Y. Ogawa, Y. Kaneko, J. P. He, X. Z. Yu, T. Arima, and Y. Tokura, Phys. Rev. Lett. **92**, 047401 (2004).

[18] M. O. Ramirez, A. Kumar, S. A. Denev, Y. H. Chu, J. Seidel, L. Martin, S.-Y. Yang, R. C. Rai, X. Xue, J. F. Ihlefeld, N. Podraza, E. Saiz, S. Lee, J. Klug, S. W. Cheong, M. J. Bedzyk, O. Auciello, J. L. Musfeldt, D. G. Schlom, R. Ramesh, J. Orenstein, and V. Gopalan, arXiv:0803.3473, Phys. Rev. B (to be published).

[19] F. Wooten, *Optical Properties of Solids* (Academic Press, New York, 1972).

[20] Absolute levels of $\alpha(E)$ underlie sample appearance: 100 nm thin films are yellow, μm-sized powders are red, and mm-sized crystals are black.

[21] J. F. Ihlefeld, N. J. Podraza, Z. K. Liu, R. C. Rai, X. Xu, T. Heeg, Y. B. Chen, J. Li, R. W. Collins, J. L. Musfeldt, X. Q. Pan, J. Schubert, R. Ramesh, and D. G. Schlom, Appl. Phys. Lett. **92**, 142908 (2008).

[22] A. Kumar, R. C. Rai, N. J. Podraza, S. Denev, M. Ramirez, Y. H. Chu, L. W. Martin, J. Ihlefeld, T. Heeg, J. Schubert, D. G. Schlom, J. Orenstein, R. Ramesh, R. W. Collins, J. L. Musfeldt, and V. Gopalan, Appl. Phys. Lett. **92**, 121915 (2008).

[23] A. J. Hauser, J. Zhang, L. Mier, R. A. Ricciardo, P. M. Woodward, T. L. Gustafson, L. J. Brillson, and F. Y. Yang, Appl. Phys. Lett. **92**, 222901 (2008).

[24] The intensity analysis is less reliable for the 1.90 eV peak because of the charge transfer absorption background.

[25] K. Huang and A. Rhys, Proc. R. Soc. London, Ser. A **204**, 406 (1950).

[26] M. K. Singh, R. S. Katiyar, and J. F. Scott, J. Phys.: Condens. Matter **20**, 252203 (2008).

[27] J. F. Scott, M. K. Singh, and R. S. Katiyar, J. Phys.: Condens. Matter **20**, 322203 (2008).

[28] Pure exciton intensities are much weaker due to their magnetic dipole nature.

[29] V. V. Eremenko and E. G. Petrov, Adv. Phys. **26**, 31 (1977).

[30] R. A. Shatwell and A. J. McCaffery, Phys. Rev. B **12**, 3815 (1975).

[31] C. Ederer, and N. A. Spaldin, Phys. Rev. B **71**, 060401(R) (2005).